MITSUBISHI ELECTRIC RESEARCH LABORATORIES
http://www.merl.com

Low Complexity TOA Estimation for Impulse Radio UWB Systems

I. Guvenc; Zafer Sahinoglu

TR2005-025 December 2005

Abstract

Due to extremely narrow pulses, an impulse radio signaling has a strong potential for high-precision positioning. Highly dispersive nature of ultra-wideband (UWB) channels makes time of arrival (TOA)estimation extremely challenging, where the leading-edge path is not necessarily the strongest path. Since the bandwidth of a received UWB signal is very large, the Nyquist rate sampling becomes impractical, hence motivating lower complexity and yet accurate ranging techniques at feasible sampling rates. In this paper, we consider TOA estimation baased on symbol rate samples that are obtained after a square-law device. Signal conditioning techniques based on wavelets and a bank of cascaded multi-scale energy collection filters are introduced, where correlations across multiple scales are exploited for edge and peak enhancements towards a more accurate detection. An adaptive threshold selection approach based on the minimum and maximum values of the energy samples is introduced, and optimal values of the thresholds for different signal to noise ratios (SNRs) are investigated via simulations. Theoreticaal closed form expressions are derived for mean absolute TOA estimation error, and compared with simulations. The performances of the discussed algorithms are tested on IEEE 802.15.4a residential line-of-sight (LOS) and non-LOS channels. Simulation results show that the introduced multi-scale energy product technique supported with a search-back step to detect the leading edge performs better than all the other techniques, excluding the pure threshold comparison algorithm at very large SNR values.

IEEE Journal on Selected Areas in Communication

Low Complexity TOA Estimation for Impulse Radio UWB Systems

I. Guvenc[1,2], Z. Sahinoglu[1]

[1]Mitsubishi Electric Research Labs, 201 Broadway Ave., Cambridge, MA, 02139

[2]Department of Electrical Engineering, University of South Florida, Tampa, FL, 33620

E-mail:{guvenc, zafer}@merl.com

Abstract

Due to extremely narrow pulses, an impulse radio signaling has a strong potential for high-precision positioning. Highly dispersive nature of ultra-wideband (UWB) channels makes time of arrival (TOA) estimation extremely challenging, where the leading-edge path is not necessarily the strongest path. Since the bandwidth of a received UWB signal is very large, the Nyquist rate sampling becomes impractical, hence motivating lower complexity and yet accurate ranging techniques at feasible sampling rates. In this paper, we consider TOA estimation based on symbol rate samples that are obtained after a square-law device. Signal conditioning techniques based on wavelets and a bank of cascaded multi-scale energy collection filters are introduced, where correlations across multiple scales are exploited for edge and peak enhancements towards a more accurate detection. An adaptive threshold selection approach based on the minimum and maximum values of the energy samples is introduced, and optimal values of the thresholds for different signal to noise ratios (SNRs) are investigated via simulations. Theoretical closed form expressions are derived for mean absolute TOA estimation error, and compared with simulations. The performances of the discussed algorithms are tested on IEEE 802.15.4a residential line-of-sight (LOS) and non-LOS channels. Simulation results show that the introduced multi-scale energy product technique supported with a search-back step to detect the leading edge performs better than all the other techniques, excluding the pure threshold comparison algorithm at very large SNR values.

I. Introduction

This decade will see a rise in location aware applications in diverse fields from asset management and home/building automation to environmental monitoring and disaster management. This wide market need recently urged emerging IEEE 802.15.4a standards workgroup (WG) to invite proposals for an alternative PHY to the existing IEEE 802.15.4 standards, requiring a sub-meter precision ranging capability. The content of this article on multi-scale non-coherent TOA estimation, has been one of the ranging proposals under consideration in IEEE 802.15.4a.

High time resolution is one of the key benefits of ultra-wideband (UWB) signals for precision ranging. Due to extremely short duration of transmitted UWB pulses, UWB receivers, as opposed to typical narrow-band wireless receivers, enjoy being able to observe individual multipath components; and the accuracy of TOA estimation is characterized by how finely the first arriving signal path is identified, which may not be the strongest.

UWB receivers typically have to operate at very low sampling rates. This makes it difficult to effectively capture the energy at each individual multipath component using Rake receivers, as it is extremely difficult to synchronize to each tap. A chip-spaced sampling of the channel can be used to detect the chip-spaced *observation* of the channel impulse response (CIR), which typically carries a fraction of the available energy of the actual CIR (such as %30 [1]). Note that higher rate samples (such as chip-rate or frame-rate) can be achieved by using symbol-spaced sampling and multiple training symbols, and shifting the signal by desired sampling period at each symbol. Another practical concern is the requirement to have a-priori knowledge of the received pulse shape for match filter implementation, which may change from an environment to another and even between different multipath components [2]. Therefore, it is difficult to exactly match to the received pulse-shape, especially when considering the analog implementations of the template waveforms.

Typical approaches for UWB ranging in the literature are based on matched filtering (MF) of the received signal. Corresponding the time index that maximizes the MF output to the TOA estimate is probably the simplest ranging technique [3]-[8]. However, these approaches have limited TOA precision, as the strongest path is not necessarily the first arriving path. In order to determine the leading edge of a received signal, Lee and Scholtz proposed to use a generalized maximum-likelihood (GML) approach to search the paths prior to the strongest path [9]. The delay and ratio statistics between the first arriving path and strongest path are obtained from extensive IEEE 802.15.3a channel measurements, and early false-alarm and missed-direct path error probabilities are derived. However, very high sampling rates

and a large memory space is required to store sample values within a search interval. Furthermore, the information included in the paths after the strongest path were neglected, which can be used to enhance strongest path detection. In [10], the leading edge detection problem is taken as a break-point estimation of the actual signal itself, where also very high sampling rate of the received signal is assumed. Temporal correlation arising from the transmitted pulse is used to accurately partition the received signal into two zero-mean Gaussian distributed time-series with different covariance matrices. In another approach, a two-step ranging algorithm is used, where an energy detection step gives coarse information about the signal's whereabouts, and a correlation based approach is applied into the detected energy block(s) for refinement [11], [12]. Timing acquisition for UWB, which in essence have many analogies with TOA estimation problem, has been extensively analyzed in the literature. Representative references include [13]-[15] and the references therein, where dirty templates and generalized likelihood ratio testing approaches were commonly used.

Due to above practical concerns and limitations, energy detection based ranging becomes more feasible. Even though it suffers more from noise due to a square-law device, energy detection does not require accurate timing or pulse shapes. Once collecting the energy samples at the output of a square-law device (which is also valid for the absolute values of the MF outputs), the TOA estimation can be considered as a problem of leading edge detection (or change/break-point detection) in noise. In this paper, we consider TOA estimation of the received signal based on symbol-rate samples, and compare the performances of maximum energy selection and threshold based approaches. New signal conditioning methods to improve detection performance based on wavelet filters and a bank of cascaded energy collection filters are introduced and analyzed via theoretical expressions and simulations. The leading edge problem has analogies with various other areas in the literature, including edge detection in image processing [16], [17], voice activity detection in speech processing [18]-[20], and spike-detection in biomedical engineering [21]-[23]. Therefore, before starting the analysis and discussion of various TOA estimation techniques, first, a brief overview of change detection algorithms will be presented in the next section.

II. A Brief Review of Change Detection Algorithms

Change detection problems have been investigated extensively in the past. When the signal statistics are known before and after the change-point, the optimal level detection can be achieved by tracking the log-likelihood ratios of the signals from the two hypothesized distributions. Cumulative sum (CUMSUM) algorithm is a popular online change detection approach, which uses a threshold on the sum of log-

likelihood ratios for the detection of the abrupt change [24]. In [25], an adaptive approach was proposed as a modification to CUMSUM algorithm for the unknown hypothesis case, which estimates the signal parameters using two sliding windows. The common case of unknown hypothesis testing problems (where the probability distribution functions (PDFs) of both hypothesis are not known) can be named as *composite hypothesis test* [26]. Two common approaches for the solution of composite hypothesis testing problems are 1) Bayesian approach, where the unknown parameters are assumed random variables with a prior PDF, and 2) Generalized likelihood ratio test (GLRT), where unknown parameters are estimated for use in a likelihood ratio test. Marginalized likelihood ratio test (MLRT) [27], [28] eliminates certain shortcomings of GLRT, dropping a requirement for a user-chosen threshold, or the knowledge of the noise statistics.

The change point detection approaches discussed above, which are based on detecting the changes in statistical distributions, typically require large number of samples [26], [29]. In typical scenarios considered under the scope of this paper, where we do not have Nyquist rate sampling, and have few samples for the detection of the leading edge, such algorithms may not be appropriate.

Considering more basic techniques, probably the simplest approach to detection of edges in a signal is passing the signal through a gradient operator (such as $[-1\ 0\ 1]$). However, this approach is not robust against noise effects, and filtered derivative techniques are commonly used for smoothing purposes for improved performance. Witkin in his pioneering work [30] developed the idea of scale-space filtering, where the signal is smoothed at various scales with Gaussians of different variances. Local minima and maxima of the derivative of the smoothed signal at various scales (which can also be obtained by filtering the initial signal with derivatives of Gaussians at various scales) then corresponds to the edges of the signal at different resolutions. Zero-crossings of the convolution of the signal with the second derivatives of Gaussians at various scales can be also used to identify the edges [31]; however, this does not give information about the direction (rising-edge vs. falling-edge), or, the sharpness of the edge. Witkin proposed a coarse-to-fine tracking of these edges in the *scale-space image* (by exploiting the correlations across the scales) to identify and localize the major singularities in the signal. Mallat *et. al.* analyzed scale-space representation of the signal in the wavelet-theory framework, and used the wavelet transform modulus maxima (WTMM) for the identification of the major edges in the signal [32], [33]. The non-orthogonal discrete wavelet transform (DWT) proposed by Mallat and Zhang (MZ) is commonly referred to as MZ-DWT in the literature [29], [34]. They showed that by analyzing the evolution of the wavelet transform exponent across scales, local Lipschitz exponent (which is a measure of the local regularity of the signal) can be estimated. Then, this allows for effective denoising of the signal using the

Lipschitz exponent and other *a-priori* information. In [35], it was proposed to use the sum of the *cone of influence* for the estimation of the regularity of the signal, which has a lower computational complexity. Alternative time-frequency approaches based on the short term Fourier transform (STFT) were considered in [36]. Stationarity index in this work was defined to be the distance between the STFTs in consecutive time windows (Kolmogorov distance was selected to be the best distance metric compared to Kullback and Jensen-like distances), and timing index that maximizes the distance was selected to be the change point. Stationarity index idea was applied to abrupt change detection of broadband signals in [37].

Before the wavelet theory gaining much popularity, the idea of using the cross-scale multiplication of sub-band decomposition of an image was first developed by Rosenfeld in [38], [39], which proved to be very efficient for locating significant edges. Xu *et. al.*, instead of using the computationally more complicated and slightly more accurate techniques of [30], [32], [40] for tracking the edges in the scale-space image (or the WTMM tree), proposed to use the direct multiplication of wavelet transform data at various scales to enhance the edges and suppress the noise [41]. The approach of using product of multi-scale wavelet coefficients has been investigated extensively in subsequent work in the literature for detection of sharp edges in the signals [29], [34], [42]-[48].

Detection of TOA of the UWB signal is equivalent to the detection of the leading-edge of the received multipath components. Typically, power delay profiles (PDP) of UWB channels are modeled with a double exponentially decaying model. On the other hand, individual multipath components are subject to Nakagami fading. Depending on the environment, the leading edge that we are trying to detect may or may not be a sharp edge. Also, considering an energy detection approach, where blocks of some arbitrary size are used to obtain energy-samples, the first arriving path may appear anywhere within a block (with a uniform distribution), which may prevent sharp edges in the energy sequence. Therefore, using solely the multi-resolution edge detection approaches discussed in previous sections may not yield as strong results.

On the other hand, the multi-resolution approach can still be used to enhance the peak-detection performance on the energy samples. In this paper, we propose to use multi-scale analysis of the received energy samples as a conditioing tool for the purposes of 1) enhancing peaks closer to the leading edge of the signal, and 2) Suppressing the noise samples. Upon more accurate estimation of samples closer to the leading edge, a search-back algorithm with a threshold detection can be used to estimate the leading edge of the signal.

III. System Model

Let the received UWB multipath signal be represented as

$$r(t) = \sum_{j=-\infty}^{\infty} d_j \omega_{mp}\big(t - jT_f - c_j T_c - \tau_{toa}\big) + n(t) \tag{1}$$

where frame index and frame duration are denoted by j and T_f, N_s represents the number of pulses per symbol, T_c is the chip duration, T_s is the symbol duration, τ_{toa} is the TOA of the received signal, and N_h is the possible number of chip positions per frame, given by $N_h = T_f/T_c$. Effective pulse after the channel impulse response is given by $\omega_{mp}(t) = \sqrt{E}\sum_{l=1}^{L} \alpha_l \omega(t - \tau_l)$, where $\omega(t)$ is the received UWB pulse with unit energy, E is the pulse energy, α_l and τ_l are the fading coefficients and delays of the multipath components, respectively. Additive white Gaussian noise (AWGN) with zero-mean and double-sided power spectral density $\mathcal{N}_0/2$ and variance σ^2 is denoted by $n(t)$. No modulation is considered for the ranging process.

In order to avoid catastrophic collisions, and smooth the power spectral density of the transmitted signal, time-hopping codes $c_j^{(k)} \in \{0,\ 1, ..., N_h - 1\}$ are assigned to different users. Moreover, random-polarity codes $d_j \in \{\pm 1\}$ are used to introduce additional processing gain for the detection of desired signal, and smooth the signal spectrum (see Fig. 1).

A. Sampling of the Received Signal After a Square-law Device

In the sequel, we assume that a coarse acquisition on the order of frame-length is acquired in (1), such $\tau_{toa} \sim \mathcal{U}(0, T_f)$, where $\mathcal{U}(.)$ denotes the uniform distribution. As for the search region, the signal within time frame T_f plus half of the next frame is considered to factor-in inter-frame leakage due to multipath, and the signal is then input to a bank of square-law devices each with an integration interval of T_b (see Fig. 2).

The number of samples (or blocks) is denoted by $N_b = \frac{3}{2}\frac{T_f}{T_b}$, and $n \in \{1,\ 2, ..., N_b\}$ denotes the sample index with respect to the starting point of the uncertainty region. With a sampling interval of t_s (which is equal to block length T_b), the sample values at the output of the square-law device are given by

$$z[n] = \sum_{j=1}^{N_s} \int_{(j-1)T_f + (c_j + n - 1)T_b}^{(j-1)T_f + (c_j + n)T_b} |r(t)|^2 dt\ , \tag{2}$$

and the performance can be further improved by using the energy in N_T symbols. The bit energy when using N_s pulses becomes $E_b = N_s E$. Note that there exists a trade-off between using larger blocks and smaller blocks in energy detection. As the block size gets narrower individual peaks due to noise

increases the likelihood of leading-energy block misdetection. Besides, there is a trade-off between using multiple pulses per symbol and a single pulse with an equivalent energy. It is well known that means and variances of non-energy and energy bearing blocks out of a square law device are given by $\mu_0 = M\sigma^2$, $\sigma_0^2 = 2M\sigma^4$, $\mu_e = M\sigma^2 + E_n$, $\sigma_e^2 = 2M\sigma^4 + 4\sigma^2 E_n$, respectively, where M is the degree of freedom given by $M = 2BT_b+1$, E_n is the total signal energy within the nth block, and B is the signal bandwidth. Let us consider two scenarios to see how these statistics will vary; the first one using a processing gain (N_s pulses per symbol) and the second one using a single pulse with the aggregate energy of all N_s pulses.

1) Single pulse per symbol: The means and variances of the non-energy and energy bearing blocks are given by $\mu_0 = M\sigma^2$, $\sigma_0^2 = 2M\sigma^4$, $\mu_e = M\sigma^2 + N_s E_n$, $\sigma_e^2 = 2M\sigma^4 + 4N_s\sigma^2 E_n$, respectively. Note that the distance between the means of noise-only blocks and energy blocks is $N_s E_n$.

2) Multiple pulses per symbol: The means and variances of the non-energy and energy bearing blocks are given by $\mu_0 = N_s M\sigma^2$, $\sigma_0^2 = 2N_s M\sigma^4$, $\mu_e = N_s\big(M\sigma^2 + E_n\big)$, $\sigma_e^2 = N_s\big(2M\sigma^4 + 4\sigma^2 E_n\big)$, respectively. When transmitting multiple pulses, even though the means of both blocks are increased due to collection of noise terms at various branches, the distance between the means of noise-only blocks and energy blocks is still $N_s E_n$. On the other hand, the variances of both noise-only blocks and energy blocks are increased. This implies that the performance when using multiple pulses per bit will be worse, and it will be better to use fewer pulses with larger power, as long as complying with local regulatory masks.

IV. TOA Estimation Algorithms

Let $z[n]$ denote the n^{th} element of length N_b energy vector after the square-law device. If multiple frames are used ($N_s > 1$), energies from same integrator positions in each frame are superposed together to obtain a single energy vector corresponding to a single frame, assuming that statistics of the channel would remain the same. In this section, various algorithms that operate on $z[n]$ values for leading edge detection are presented and formulated. Some of the basic algorithms to be discussed are depicted in Fig. 3.

A. Maximum Energy Selection (MES)

Choosing the maximum energy output to be the leading edge is the simplistic way of achieving a TOA estimation. Using MES, the TOA estimate with respect to the beginning of the time frame is evaluated as $\hat{t}_{MES} = \Big[\underset{1\le n\le N_b}{\operatorname{argmax}}\big\{z[n]\big\}\Big]T_b = n_{max}T_b$. However, the strongest energy block in many cases may not

be the leading energy block (Fig. 3), and the MES therefore hits an error-floor even in high signal to noise ratio (SNR) region. Also, the performance of it degrades with N_b, since it becomes more likely to identify a noise only block as the maximum energy block.

B. Threshold Comparison (TC)

Received samples can be compared to an appropriate threshold, and the first threshold-exceeding sample index can be corresponded as the TOA estimate, i.e. $\hat{t}_{TC} = \Big[\min\big\{n|z[n] > \xi\big\}\Big] T_b$, where ξ is a threshold that must be set based on the received signal statistics. Given the minimum and maximum energy sample values, the following normalized adaptive threshold can be used (see Fig. 4)

$$\xi_{norm} = \frac{\xi - \min\{z[n]\}}{\max\{z[n]\} - \min\{z[n]\}} \ . \tag{3}$$

Optimal value of ξ_{norm} changes depending on the SNR as discussed later in the paper.

C. Maximum Energy Selection with Search-Back (MES-SB)

In order to improve the performance of the TC in low SNRs, the energy samples prior to the maximum should be searched. The TOA estimate with a thresholding and backward search is then given by $\hat{t}_{MES-SB} = \Big[\min\{n|\tilde{z}[n] < \xi\} + n_{max} - W_{sb} - 1\Big] T_b$, where $\tilde{z}[n] = \Big[z[n_{max} - W_{sb}] \ z[n_{max} - W_{sb} + 1] \ \ ... \ \ z[n_{max}]\Big]$. Search-back window is denoted by W_{sb}, which is set based on the statistics of the channel, and is $\lceil 15\text{ns}/T_b \rceil$ in our simulations. Note that the accuracy of this approach is also limited by the accuracy of the MES.

D. Weighted Multiscale Product (WMP) of MZ-DWT

Derivative of Gaussian (dG) approaches are commonly used in the literature for detecting the edges by analyzing the signal at multiple scales, where in order to preserve the correlation (and regularities) across various scales, non-orthogonal MZ-DWT [33] is employed. The MZ-DWT of $z[n] \in L^2(\mathcal{R})$ at scale s, where $1 \leq n \leq N_b$, is given by

$$W_{2^s} z[n] = z[n] * \phi_{2^s}[n] = \sum_m \phi_{2^s}[m] z[n-m] \ , \tag{4}$$

which is equivalent to

$$W_{2^s} z[n] = \left(z * \left(2^s \frac{d\psi_{2^s}}{dn} \right) \right)[n] = 2^s \frac{d}{dn} \big(z * \psi_{2^s} \big)[n] \ , \tag{5}$$

where $\psi[n]$ and $\phi[n]$ are discrete-time approximations to the Gaussian function and its derivative using cubic and quadratic splines, respectively, $*$ denotes convolution, $1 \leq s \leq S-1$, and $S = \log_2 N_b$.

Equation (5) implies that MZ-DWT is analogous to smoothing the signal with Gaussian splines at multiple scales and then estimating the gradients.

As analyzed by Sadler *et. al.* in [29], [34], multiscale product (MP) of MZ-DWT given by

$$P_{S_{opt}}^{(DWT)}[n] = \prod_{s=1}^{S_{opt}} W_{2^s} z[n] \ , \tag{6}$$

can be effectively used for improving the accuracy of edge detection, where S_{opt} is the optimal scale that enhances the regularities. However, it is not guaranteed to observe sharp edges in the UWB energy vector, and since the energy samples do not have a smooth variation, the edges can be mixed with noise samples when the MP-MZ-DWT is used. Poor edge detection performance of this approach in our simulations (which is not surprising due to the discussed issues) motivated us to introduce a weighting function to suppress the edges caused by noise while promoting the edges in the vicinity of the energy-bearing blocks.

$$\tilde{P}_{S_{opt},\zeta}^{(DWT)}[n] = \underbrace{\Big(\psi_{2^\zeta}[n] - \min\big\{\psi_{2^\zeta}[n]\big\}\Big)}_{\text{Weighting Function } = G(\zeta)} \times \prod_{s=1}^{S_{opt}} W_{2^s} z[n] \ , \tag{7}$$

where ζ is an arbitrary scale so that the energy in the multipath delay profile is effectively captured in the smoothed signal. The value of ζ is set to 3 in our simulations. The TOA estimate is then given as $\hat{t}_{DWT} = \Big[\underset{1\le n\le N_b}{\text{argmax}}\big\{\tilde{P}_{S_{opt},\zeta}^{(DWT)}[n]\big\}\Big] T_b$ for n even, and $\hat{t}_{DWT} = \Big[\underset{1\le n\le N_b}{\text{argmin}}\big\{\tilde{P}_{S_{opt},\zeta}^{(DWT)}[n]\big\}\Big] T_b$ for n odd (with the distinction arising in order to calculate the rising edge).

V. Improving the Accuracy of MES

In this section two filtering techniques that enhance the accuracy of maximum energy block selection are presented. The first uses the average energy distribution around the maximum energy block, while the second a bank of scaling filters designed in a dyadic tree structure, which improves the maxima closer to the leading edge of the signal.

A. Filtered Maximum Energy Selection (F-MES)

By knowing the average energy distribution around the maximum energy block, one can filter the energy vector to enhance the peaks (and suppress noise components) by collecting the energies present in the neighboring blocks. In Fig. 6 the mean energy distribution around the maximum energy block is shown for $T_b = 1$ns and $T_b = 4$ns, after averaging over 1000 channel realizations for CM1. The mean block energy values are not significantly different for CM2, and therefore those figures are not included here. In order to capture the energy effectively and characterize the peaks better, one can filter

the received energy vector with a time-reversed form of the discrete data in Fig. 6, and then apply the MES-SB or another algorithm to determine the leading edge.

B. Multiscale Energy Products (MEP)

Signal energies from coarse to finer time scales can be exploited to improve leading edge detection performance. Since the energy values at different scales would be correlated, their product is expected to enhance the peaks due to signal existence.

Let $h_{2^s}[n]$ denote the rectangular filter at scale s, given by

$$h_{2^s}[n] = u[n + 2^s] - u[n] \ , \tag{8}$$

where $s = 1, 2, ..., S$ is the scale number ranging from finer scales to coarser, $S = \lfloor \log_2 N_b \rfloor$, and $u[n]$ is the step function. The convolution of $h_{2^s}[n]$ with the energy vector $\underline{z}$ produces energy concentration of our signal at various scales, given by

$$y_s[n] = \sum_k z[k] h_{2^s}[n - k]. \tag{9}$$

Since $y_s[n]$ are correlated across different scales, we can use their direct multiplication to enhance the peaks closer to the leading edge of the signal, and suppress noise components, i.e.

$$P_S^{(MEP)}[n] = \prod_{s=1}^{S} y_s[n], \tag{10}$$

where $P_S^{(MEP)}[n]$ denotes the product of convolution outputs from scale 1 (which is the energy vector itself) through scale S. Then, the location of the strongest path is estimated as $\hat{t}_{MEP} = \Big[\underset{1 \le n \le N_b}{\operatorname{argmax}} \big\{ P_S[n] \big\}\Big] T_b$. Note that once the strongest energy block is estimated, a search-back algorithm can be run to detect the leading edge of the signal more accurately.

VI. Error Analysis for TC Based TOA Estimation

In this section, mean absolute error (MAE) of the TC based TOA estimation is analyzed, and closed form error expressions are presented. First, the probability of detection of a certain block is derived, which leads us to the derivation of MAE of the TOA estimate for the case of uniformly distributed TOA. Assume initially that the delay of the leading-edge energy block is fixed. Let n_{toa} denote the first arriving energy block index, $\hat{n}$ denote the estimated block index, and $n = 1, 2, \cdots, N_B$ denote the block indices

where the energy block is being searched. Then, fixing the value of threshold ξ, probability of detecting an arbitrary block n_{hyp} to be the energy block is calculated as[1]

$$\begin{aligned} P_D(n_{hyp}) &= P(\hat{n} = n_{hyp}) \\ &= \Bigg[\prod_{n=1}^{n_{hyp}-1} P\big(z[n] < \xi\big) \Bigg] \times P\big(z[n_{hyp}] > \xi\big) \ , \end{aligned} \tag{11}$$

where $z[n]$ has a centralized Chi-square distribution for $n = 1, 2, \cdots, n_{toa} - 1$ (corresponding to noise-only blocks), and non-centralized Chi-square distribution for $n = n_{toa}$. The cumulative distribution functions (CDFs) of these centralized and non-centralized Chi-square random variables are given by

$$\begin{aligned} P_{chi2}(\xi) &= P\big(z[n] < \xi\big) \\ &= 1 - \exp\left(-\frac{\xi}{2\sigma^2}\right) \sum_{l=0}^{M/2-1} \frac{1}{l!} \left(\frac{\xi}{2\sigma^2}\right)^2 \end{aligned} \tag{12}$$

$$P_{ncx2}(E_n, \xi) = P\big(z[n] < \xi\big) = 1 - Q_{M/2}\left(\frac{E_n}{\sigma}, \frac{\sqrt{\xi}}{\sigma}\right) \ , \tag{13}$$

where $\sigma^2 = \frac{N_0}{2}$ is the noise variance, $Q_x(.)$ denotes the Marcum-Q function with parameter x, and E_n is the signal energy within the nth block, whose PDF varies with n, block size, and channel model. Note that $n_{hyp} = n_{toa}$ corresponds to correct detection, and the probability of falsely detecting the first energy block is simply calculated as $P_{FD}(n_{toa}) = P\big(\hat{n} \neq n_{toa}\big) = 1 - P_D\big(n_{toa}\big)$. Fixing the value of ξ, three cases can be considered for n_{hyp}. If $n_{hyp} < n_{toa}$,

$$P_D(n_{hyp}) = [P_{chi2}(\xi)]^{n_{hyp}-1}\big(1 - P_{chi2}(\xi)\big) \ , \tag{14}$$

while on the other hand if $n_{hyp} = n_{toa}$,

$$\begin{aligned} P_D(n_{hyp}) &= [P_{chi2}(\xi)]^{n_{toa}-1} \times \\ &\int_{E_{n_{toa}}} \Big(1 - P_{ncx2}(E_{n_{toa}}, \xi)\Big) p(E_{n_{toa}}) dE_{n_{toa}} \ , \end{aligned} \tag{15}$$

If $n_{hyp} > n_{toa}$, we can further consider two conditions. Let N_{eb} denote the number of noise plus energy blocks where there exists a significant amount of energy. If $n_{hyp} - n_{toa} < N_{eb}$

$$\begin{aligned} P_D(n_{hyp}) &= [P_{chi2}(\xi)]^{n_{toa}-1} \Bigg(\prod_{n=n_{toa}}^{n_{hyp}-1} \int_{E_n} P_{ncx2}(E_n, \xi) p(E_n) dE_n \Bigg) \\ &\times \int_{E_{n_{hyp}}} \Big(1 - P_{ncx2}(E_{n_{hyp}}, \xi)\Big) p(E_{n_{hyp}}) dE_{n_{hyp}} \ , \end{aligned} \tag{16}$$

[1]Note that this is valid for $n_{hyp} \geq 2$. For $n_{hyp} = 1$, the terms corresponding to noise blocks become unity.

while, if $n_{hyp} - n_{toa} \geq N_{eb}$

$$P_D(n_{hyp}) = [P_{chi2}(\xi)]^{n_{hyp}-N_{eb}-1}\Big(1 - P_{chi2}(\xi)\Big) \times \prod_{n=n_{toa}}^{n_{toa}+N_{eb}-1} \int_{E_n} P_{ncx2}(E_n, \xi) p(E_n) dE_n \ . \tag{17}$$

In order to carry out the evaluation of the detection probabilities, the energy PDFs $p(E_n)$ are obtained via simulations (see Fig. 11) with considering the uniformly distributed delay offsets of the individual paths within the blocks. Note that in order to calculate closed form expressions for the detection probabilities in the case of normalized thresholds presented in (3) rather than fixed thresholds, the PDFs of ξ_{norm} can be used. However, our simulations show that especially for large E_b/N_0 values, ξ_{norm} is highly correlated with the energies in the first couple of energy blocks, with correlation coefficients being on the order of 0.6 at $E_b/N_0 = 26dB$ for the first four energy plus noise blocks. This implies that the PDFs of ξ_{norm} also has to be conditioned on E_n, which makes closed form error analysis cumbersome and analytically intractable for variable ξ.

Now let $n_{toa} \sim \mathcal{U}(1, N_B)$. After averaging over different block offsets, the probability of correct detection of first energy block becomes

$$\begin{aligned} P_D^{(avg)}\big(n_{toa}\big) &= \sum_{n_{toa}=1}^{N_B} P_D\big(n_{toa}\big) p(n_{toa}) \\ &= \frac{1}{N_b} \sum_{n_{toa}=1}^{N_B} P_D\big(n_{toa}\big) \ . \end{aligned} \tag{18}$$

whereby the average false detection probability becomes $P_{FD}^{(avg)}\big(n_{toa}\big) = 1 - P_D^{(avg)}\big(n_{toa}\big)$.

Given n_{toa} to be fixed, the MAE can be calculated by averaging over the probability of detection of different TOA estimations

$$e_{abs}[n_{toa}] = E\Big[\big|\hat{n} - n\big|\Big] = \sum_{n=1}^{N_b} P_D(n) \times \big|n - n_{toa}\big| \ . \tag{19}$$

In other words, the absolute error corresponding to each block are weighted by the probability of detecting that particular block. For $n_{toa} \sim \mathcal{U}(1, N_B)$, we can average $e_{abs}[n_{toa}]$ to obtain the average error as

$$e_{abs}^{(avg)} = \sum_{n_{toa}=1}^{N_b} e_{abs}[n_{toa}] p(n_{toa}) = \frac{1}{N_b} \sum_{n_{toa}=1}^{N_b} e_{abs}[n_{toa}] \ . \tag{20}$$

It is worth to mention that given the means and variances of the centralized and non-centralized Chi-square distributions as $\mu_0[n] = M\sigma^2$, $\sigma_0^2[n] = 2M\sigma^4$, $\mu_e[n] = M\sigma^2 + E_n$, $\sigma_e^2[n] = 2M\sigma^4 + 4\sigma^2 E_n$, we can use Gaussian approximation (for appropriately large values of M) to model the received signal

statistics. Then, the approximated CDF will be given by $\tilde{P}_{chi2}(\xi) = Q\left(\frac{\xi-\mu_0[n]}{\sigma_0[n]}\right)$ for the noise only blocks, and $\tilde{P}_{ncx2}(E_n, \xi) = Q\left(\frac{\xi-\mu_e[n]}{\sigma_e[n]}\right)$ for the energy plus noise blocks.

VII. IEEE 802.15.4A CHANNEL MODELS

In all the simulations that are presented in the next section, the channel models CM1 (residential LOS) and CM2 (residential NLOS) of IEEE802.15.4a [49] are employed (Fig. 8). The channel realizations are sampled at 8GHz, 1000 different realizations are generated, and each realization has a TOA uniformly distributed within $(0, T_f)$. In IEEE 802.15.4a residential environment channel measurements, tap-amplitude statistics are reported to be Rayleigh distributed as opposed to log-normal in IEEE 802.15.3a. Mean number of clusters in CM1 is 3 and while in CM2 it is 3.5.

A raised cosine pulse of $T_c = 1$ns is considered for all scenarios, and it is convolved with the realizations of both CM1 and CM2 channels to obtain the received signal. After introducing uniformly distributed delays, energies are collected within non-overlapping windows to obtain decision statistics. Two critical statistics for the accuracy of the TOA estimation at this step are the PDF of the energy of the maximum energy block (Fig. 9), and the PDF of the delay between the maximum energy block and the leading edge block (Fig. 10). Since CM2 is a non-LOS channel, its delay spread is expectedly longer than that of CM1. Therefore, as typically observed, it would be more likely for the highest energy blocks in CM2 to have less energy compared to the highest energy blocks in CM1, when the total received energy is normalized. Also in Fig. 11, PDFs of the energies within the first four blocks including and after the leading edge block are presented. These PDFs are used to evaluate the theoretical expressions derived in previous section, as will be compared with simulations in the next section.

The other simulation parameters are (unless otherwise stated) $T_f = 200$ns, $B = 4$GHz, $N_T = 1$, and $N_s = 1$. Both 1ns and 4ns are considered for T_b. The MAE is used to compare the performances of different algorithms. However, although the large frame interval chosen in our simulations considerably increases the MAE (such as due to choosing the noise only blocks in MES based algorithms), the fact that there exists consecutive energy plus noise blocks yields clusterings of the delay errors at and after the n_{toa}th block (see Fig. 15). This implies that small TOA estimates greater than t_{toa} have larger confidence values. Note that each 1ns timing error corresponds to 33cm of ranging error as can be calculated from the speed of light.

VIII. Results and Discussion

A. Normalized Threshold Characteristics of CM1 and CM2

TOA estimation errors in number of blocks with respect to the employed normalized threshold for various E_b/N_0 are given in Fig. 12 for CM1 and in Fig. 13 for CM2. It is observed that selecting ξ_{norm} to be on the order of 0.8 will yield near optimal performance at almost every E_b/N_0 under CM2, while for CM1 it must be closer to 0.2 at high E_b/N_0. Regardless of the threshold selection, at $E_b/N_0 < 20dB$ the MAE becomes intolerably high for sub-meter resolution ranging. The optimal threshold levels for CM1 and CM2 with respect to E_b/N_0 are depicted in Fig 14 for better visualization, for $T_b = 1$ns and $T_b = 4$ns.

B. Signal Peak Enhancement with MEP

The performance of the MEP method can be measured by analyzing the the decrease in the delay (compared with MES) between the strongest energy block and first energy block. Let Δ be the distance in terms of the number of blocks between first-arriving energy block and maximum energy block. Using the MEP, the peaks away from the leading edge are effectively suppressed, decreasing Δ. In Fig. 15, CDFs of Δ before and after the bank of multiscale filters are shown for $T_b = 4$ns at various E_b/N_0. It is observed that especially when the noise variance is high, the MEP lowers Δ, and consequently the error in the TOA estimate. Low E_b/N_0 also yields erroneous selection of the maximum energy block prior to the leading edge.

C. Comparison of Performances of Various TOA Estimation Algorithms

In Figs. 16-19, the performances of different energy detection based TOA estimation algorithms are tested in IEEE 802.15.4a CM1 and CM2 (which can also be implemented with absolute values of correlator outputs). The ξ_{opt} is set to $0.5(\min\{z[n]\} + \max\{z[n]\})$ with the assumption that there is no SNR estimate available, and analysis of adaptive selection of the optimal threshold is left to a subsequent discussion in the next sections. It is observed that the TC performs well at high E_b/N_0, while the MES is better at higher noise variance. The reason for TC performing poorly in general at low SNR region is frequent threshold exceedings caused by noise. On the other hand, when the SNR is large, the TC does not face an early error floor as opposed to the MES. The WMP-MZ-DWT performs better than the MES for CM1 at high E_b/N_0, however, not as well as the MES-SB. Under CM2, performance of the WMP-MZ-DWT is not acceptable. The performance improvement that comes with F-MES is better

at higher noise variance, and at larger block sizes. On the other hand, MEP and especially MEP-SB performs well at all E_b/N_0, and does not require estimation of the filter function as in the F-MES case.

The performance difference under CM1 and CM2 is over 6dB in favor of CM1 for low to moderate SNR ranges. This can be explained by Fig. 9, where the probability of large energy values is shown to be much larger for CM1 compared to CM2. On the other hand, once the TOA estimation errors hit the error floor, algorithms perform slightly better under CM2 than CM1. The explanation for this phenomena comes with Fig. 10, where it is indicated that even though the energy values are small, they are more frequently closer to the leading edge for CM2.

D. Effect of Number of Blocks on the Performance of MES

If a larger number of blocks are used in the MES, it becomes more likely that noise samples can be erroneously selected as the maximum energy block. In Fig. 20, MAE performance of MES was analyzed for various frame durations while $T_b = 1$ns. Even though there is not much variation in the performance at large E_b/N_0, higher N_b may degrade the performance at lower E_b/N_0. Also note that the selection of $N_b * T_b$, that is T_f, limits the maximum measurable distance. For instance, a distance that it would take $(N_b + 1) * T_b$ seconds for the radio frequency (RF) signal to traverse would be erroneously treated as a signal arriving within the first block in the energy analysis.

E. Comparison of Performances Using a Single Pulse, Multiple Pulses, or Multiple Symbols

In Sections III-A.1 and III-A.2, it was noted that using multiple pulses degrades the performance of TOA estimation with energy detection. In order to support this via simulations, in Fig. 21, performance of MEP-SB was studied when $N_s = 1$ and $N_s = 5$, with identical symbol energies in both cases. It is observed that using multiple pulses per symbol in essence degrades the performance with an energy detection approach. It can also be seen that multiple symbols can be used to obtain a gain at low E_b/N_0; however, at high SNR in all the cases, similar error floors are experienced.

F. Comparison of TC Based TOA Estimation Using Theory and Simulations

The theoretical and simulated performances of threshold based TOA estimators when using a fixed threshold of $0.1 \times E_b$ at all E_b/N_0 are given in Fig. 22 for CM1 ($T_b = 4$ns). The PDFs obtained via simulations in Fig. 11 are used to average the performances over the energy distributions. The PDFs of the first 8 blocks including and after n_{toa} are included only, considering the rest of the blocks to be noise-only blocks. Even though the error expression in (20) shows a good match with simulation at low

E_b/N_0 (where the ranging error is unacceptably bad), it yields optimistic results compared to simulations at large E_b/N_0.

The performance of the threshold based TOA estimation can be improved using an adaptive threshold, as discussed in previous sections. Given $\max\{z[n]\}$ and $\min\{z[n]\}$, optimum adaptive normalized threshold values that corresponds to the operated E_b/N_0 can be used to have a superior performance compared to a fixed threshold (excluding very high SNRs). However, this requires estimation of the SNR, which is not an easy task in UWB due to extremely low power operation characteristics. Instead, an adaptive normalized threshold ξ_{norm} can be used at all SNR values. As an example, $\xi_{norm} = 0.5$ is used in Fig. 22, which shows to match with the optimum threshold results at $E_b/N_0 = 22$dB, and performs suboptimal otherwise.

As a final remark, at $E_b/N_0 = 26$dB, it is observed that a fixed threshold performs better than the optimal adaptive threshold. This is due to the fact that optimal threshold values obtained via simulations are optimal *given* the knowledge of only $\max\{z[n]\}$ and $\min\{z[n]\}$. The fixed threshold values used for demonstrating theoretical and simulation results in Fig. 22 assumes the knowledge of the received energy value, which is not exploited in the adaptive threshold estimation.

IX. Conclusion

Various TOA estimation algorithms for low sampling rate UWB systems based on energy detection are analyzed. Maximum energy selection based TOA estimation is shown to be not accurate enough, particularly when the number of blocks is large. Two filtering techniques are introduced to improve the accuracy of the maximum energy selection. The first approach exploits the mean energy around the maximum energy samples in order to enhance the peaks; however, this requires a-priori knowledge of the filter shape. On the other hand, the second approach analyzes the energy at multiple time resolutions with hierarchically designed filters, so that the peaks closer to the leading edge are enhanced. Simulations show that the introduced multi-scale energy product approach implemented with a search-back step outperforms all the other algorithms in all test cases except TC algorithm at very high SNR. A comparison of using single pulse versus multiple pulses is discussed, and it is supported via simulations that using larger number of pulses actually degrades the TOA accuracy when energy detection is used.

An adaptive threshold selection approach that makes use of the minimum and maximum energy samples is introduced, and optimum threshold values are demonstrated via simulations for CM1 and CM2 channels. Closed form expressions for MAE for the fixed threshold case are derived and compared with simulations, yielding good match at low to moderate E_b/N_0 ranges.

It may be interesting to further evaluate some of the techniques discussed in the Section II, such as composite hypothesis testing and stationary index based algorithms, as they can be applied to UWB TOA estimation. Even though multi-scale products of MZ-DWT of the energy vectors did not yield as satisfactory performance in our simulations, leading edge detection techniques upon estimation of the Lipschitz exponent of the energy samples and using the WTMM can be looked into. Also, how transmitted reference schemes can be exploited for TOA estimation has not been addressed in the literature, and can be an attractive research topic.

ACKNOWLEDGEMENT

The authors would like to thank Dr. A. F. Molisch for his comments and suggestions.

REFERENCES

[1] I. Guvenc and H. Arslan, "UWB channel estimation with various sampling rate options," in *Proc. IEEE Sarnof Symposium (To Appear)*, Princeton, NJ, Apr. 2005.

[2] R. Qiu, "A study of the ultra-wideband wireless propagation channel and optimum UWB receiver design," *IEEE J. Select. Areas Commun.*, vol. 20, no. 9, pp. 1628–1637, Dec. 2002.

[3] W. Chung and D. Ha, "An accurate ultra wideband (UWB) ranging for precision asset location," in *Proc. IEEE Conf. Ultrawideband Syst. Technol. (UWBST)*, Reston, VA, Nov. 2003, pp. 389–393.

[4] B. Denis, J. Keignart, and N. Daniele, "Impact of NLOS propagation upon ranging precision in UWB systems," in *Proc. IEEE Conf. Ultrawideband Syst. Technol. (UWBST)*, Reston, VA, Nov. 2003, pp. 379–383.

[5] K. Yu and I. Oppermann, "Performance of UWB position estimation based on time-of-arrival measurements," in *Proc. IEEE Conf. Ultrawideband Syst. Technol. (UWBST)*, Kyoto, Japan, May 2004, pp. 400–404.

[6] ——, "UWB positioning for wireless embedded networks," in *Proc. IEEE Radio Wireless Conf. (RAWCON)*, Atlanta, GA, Sept. 2004, pp. 459–462.

[7] A. Rabbachin and I. Oppermann, "Synchronization analysis for UWB systems with a low-complexity energy collection receiver," in *Proc. IEEE Conf. Ultrawideband Syst. Technol. (UWBST)*, Kyoto, Japan, May 2004, pp. 288–292.

[8] R. Fleming, C. Kushner, G. Roberts, and U. Nandiwada, "Rapid acquisition for ultra-wideband localizers," in *Proc. IEEE Conf. Ultrawideband Syst. Technol. (UWBST)*, Baltimore, MD, May 2002, pp. 245–249.

[9] J.-Y. Lee and R. A. Scholtz, "Ranging in a dense multipath environment using an UWB radio link," *IEEE J. Select. Areas Commun.*, vol. 20, no. 9, pp. 1677–1683, Dec. 2002.

[10] C. Mazzucco, U. Spagnolini, and G. Mulas, "A ranging technique for UWB indoor channel based on power delay profile analysis," in *Proc. IEEE Vehic. Technol. Conf. (VTC)*, Los Angeles, CA, Sep. 2004, pp. 2595–2599.

[11] S. Gezici, Z. Sahinoglu, H. Kobayashi, H. V. Poor, and A. F. Molisch, "A two-step time of arrival estimation algorithm for impulse radio ultrawideband systems," Antalya, Turkey, Sep. 2005.

[12] S. Gezici, Z. Sahinoglu, H. Kobayashi, and H. V. Poor, *Ultra Wideband Geolocation*. John Wiley & Sons, Inc., 2005, in Ultrawideband Wireless Communications.

[13] Z. Tian, L. Yang, and G. B. Giannakis, "Symbol timing estimation in ultra wideband communications," in *Proc. IEEE Asilomar Conf. Signals Syst. Comp.*, vol. 2, Pacific Grove, CA, Nov. 2002, pp. 1924–1928.

[14] Z. Tian and G. B. Giannakis, "A GLRT approach to data-aided timing acquisition in UWB radios – Part I: Algorithms," *IEEE Trans. Wireless Commun.*, 2005 (to appear).

[15] Z. Tian and L. Wu, "Timing acquisition with noisy template for ultra-wideband communications in dense multipath," *EURASIP J. Applied Signal Processing*, Apr. 2005 (to appear).

[16] J. Canny, "A computational approach to edge detection," *IEEE Trans. Pattern Anal. Machine Intell.*, vol. 8, pp. 679–698, 1986.

[17] H. Moon, R. Chellappa, and A. Rosenfeld, "Optimal edge-based shape detection," *IEEE Trans. Image Processing*, vol. 11, no. 11, pp. 1209–1227, Nov. 2002.

[18] S. G. Tanyer and H. Ozer, "Voice activity detection in nonstationary noise," *IEEE Trans. Speech and Audio Processing*, vol. 8, no. 4, pp. 478–482, July 2000.

[19] A. Q. Z. Qi Li; Jinsong Zheng; Tsai, "Robust endpoint detection and energy normalization for real-time speech and speaker recognition," *IEEE Trans. Speech and Audio Processing*, vol. 10, no. 3, pp. 146–157, Mar. 2002.

[20] J. Sohn, N. S. Kim, and W. Sung, "A statistical model-based voice activity detection," *IEEE Signal Processing Lett.*, vol. 6, no. 1, pp. 1–3, Jan. 1999.

[21] Z. Nenadic and J. W. Burdick, "Spike detection using the continuous wavelet transform," *IEEE Trans. Biomedical Engineering*, vol. 52, no. 1, pp. 74–87, Jan. 2005.

[22] S. Mukhopadhyay and G. C. Ray, "A new interpretation of nonlinear energy operator and its efficacy in spike detection," *IEEE Trans. Biomedical Engineering*, vol. 45, no. 2, pp. 180–187, Feb. 2002.

[23] C. Li, C. Zheng, and C. Tai;, "Detection of ECG characteristic points using wavelet transforms," *IEEE Trans. Biomedical Engineering*, vol. 42, no. 1, pp. 21–28, Jan. 1995.

[24] M. Baseville and I. V. Nikiforov, *Detection of Abrupt Changes, Theory and Application*. Englewood Cliffs, NJ: Prentice-Hall, 1993.

[25] W. E. Falao, M. Khalil, and J. Duchene, "Adaptive approach for change detection in EMG recordings," in *Proc. IEEE Int. Conf. Engineering in Medicine and Biology Society*, vol. 2, Istanbul, Turkey, Oct. 2001, pp. 1875–1878.

[26] S. M. Kay, *Fundamentals of Statistical Signal Processing: Detection Theory*. Upper Saddle River, NJ: Prentice Hall, Inc., 1998.

[27] F. Gustafsson, "The marginalized likelihood ratio test for detecting abrupt changes," *IEEE Trans. Automatic Control*, vol. 41, no. 1, pp. 66–78, Jan. 1996.

[28] ——, *Adaptive Filtering and Change Detection*. John Wiley & Sons, Ltd, 2000.

[29] B. M. Sadler, T. Pham, and L. C. Sadler, "Optimal and wavelet based shockwave detection and estimation," *J. Acoust. Soc. Amer.*, vol. 104, no. 2, pp. 955–963, Aug. 1998.

[30] A. Witkin, "Scale-space filtering: A new approach to multi-scale description," in *Proc. IEEE Int. Conf. Acoust., Speech, Signal Processing (ICASSP)*, vol. 9, San Diego, CA, Mar. 1984, pp. 150–153.

[31] H. Dehghan, "Zero-crossing contour construction for scale-space filtering," in *Proc. IEEE Asilomar Conf. Signals, Systems, Computers*, vol. 2, Pacific Grove, CA, Nov. 1997, pp. 1479–1482.

[32] A. Mallat and W. L. Hwang, "Singularity detection and processing with wavelets," *IEEE Trans. Information Theory*, vol. 38, no. 2, pp. 617–643, Mar. 1992.

[33] A. Mallat and S. Zhong, "Characterization of signals from multiscale edges," *IEEE Trans. Pattern Analysis and Machine Intelligence*, vol. 14, no. 2, pp. 710–732, July 1992.

[34] B. M. Sadler and A. Swami, “Analysis of multiscale products for step detection and estimation,” *IEEE Trans. Information Theory*, vol. 45, no. 3, pp. 1043–1051, Apr. 1999.

[35] T. C. Hsung and D. P. K. Lun, “Denoising by singularity rejection,” in *Proc. IEEE Int. Symp. Circuits and Systems (ISCAS)*, vol. 1, Hong Kong, June 1997, pp. 205–208.

[36] H. Laurent and C. Doncarli, “Stationarity index for abrupt changes detection in the time-frequency plane,” *IEEE Signal Processing Lett.*, vol. 5, no. 2, pp. 43–45, Feb. 1998.

[37] J. M. Smulko, “Abrupt changes detection of broad-band signals,” in *Proc. IEEE Instrumentation Measurement Technol. Conf. (IMTC)*, vol. 2, Budapest, Hungary, May 2001, pp. 1139–1142.

[38] A. Rosenfeld, “A non-linear edge detection technique,” *IEEE Proc.*, vol. 58, no. 5, pp. 814–816, 1970.

[39] A. Rosenfeld and M. Thurston, “Edge and curve detection for visual scene analysis,” *IEEE Trans. Comput.*, vol. 20, pp. 562–569, 1971.

[40] J. Lu, J. B. Weaver, D. M. Healy, and Y. Xu, “Noise reduction with a multiscale edge representation and perceptual criteria,” in *Proc. IEEE Int. Symp. Time-Frequency and Time-Scale Analysis*, Victoria, BC, Oct. 1992, pp. 555–558.

[41] Y. Xu, J. B. Weaver, D. M. Healy, and J. Lu, “Wavelet transform domain filters: a spatially selective noise filtration technique,” *IEEE Trans. Image Processing*, vol. 3, no. 6, pp. 747–758, July 1994.

[42] A. Swami and B. M. Sadler, “Step-change localization in additive and multiplicative noise via multiscale products,” in *Proc. IEEE Asilomar Conf. Signals, Systems, Computers*, vol. 1, Pacific Grove, CA, Nov. 1998, pp. 737–741.

[43] B. M. Sadler and A. Swami, “On multiscale wavelet analysis for step estimation,” in *Proc. IEEE Int. Conf. Acoust., Speech, Signal Processing (ICASSP)*, vol. 3, Seattle, WA, May 1998, pp. 1517–1520.

[44] S. MacDougall, A. K. Nandi, and R. Chapman, “Multiresolution and hybrid Bayesian algorithms for automatic detection of change points,” *IEE Proceedings- Vision, Image, and Signal Processing*, vol. 145, no. 4, pp. 280–286, Aug. 1998.

[45] J. Ge and G. Mirchandani, “Softening the multiscale product method for adaptive noise reduction,” in *Proc. IEEE Asilomar Conf. Signals, Systems, Computers*, vol. 2, Pacific Grove, CA, Nov. 2003, pp. 2124–2128.

[46] L. Zhang and P. Bao, “A wavelet-based edge detection method by scale multiplication,” in *Proc. IEEE Int. Conf. Pattern Recognition*, vol. 3, Quebec City, Canada, Aug. 2002, pp. 501–504.

[47] M. Beauchemin and K. B. Fung, “Investigation of multiscale product for change detection in difference images,” in *Proc. IEEE Int. Geoscience and Remote Sensing Symp. (IGARSS)*, vol. 6, Anchorage, AK, Sept. 2004, pp. 3853–3856.

[48] P. Bao and L. Zhang, “Noise reduction for magnetic resonance images via adaptive multiscale products thresholding,” *IEEE Trans. Medical Imaging*, vol. 22, no. 9, pp. 1089–1099, Sept. 2003.

[49] A. F. Molisch, K. Balakrishnan, C. C. Chong, S. Emami, A. Fort, J. Karedal, J. Kunisch, H. Schantz, U. Schuster, and K. Siwiak, “IEEE 802.15.4a channel model - final report,” Sept., 2004. [Online]. Available: http://www.ieee802.org/15/pub/TG4a.html

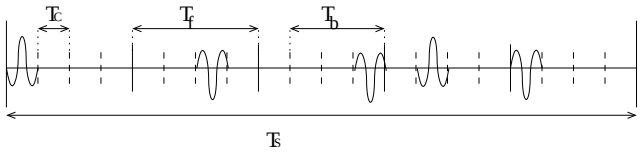

Fig. 1. Transmitted UWB-IR pulses in a symbol, where $(N_s, N_h) = (5, 4)$, $T_b = 3T_c$, and $\big(\{c_j\}, \{d_j\}\big) = \big(\{0, 2, 3, 1, 0\}, \{+1, -1, -1, +1, -1\}\big)$.

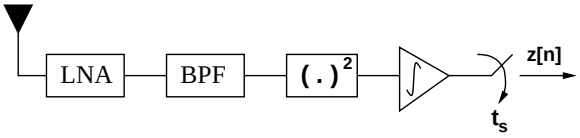

Fig. 2. Sampling of the received signal after energy detection.

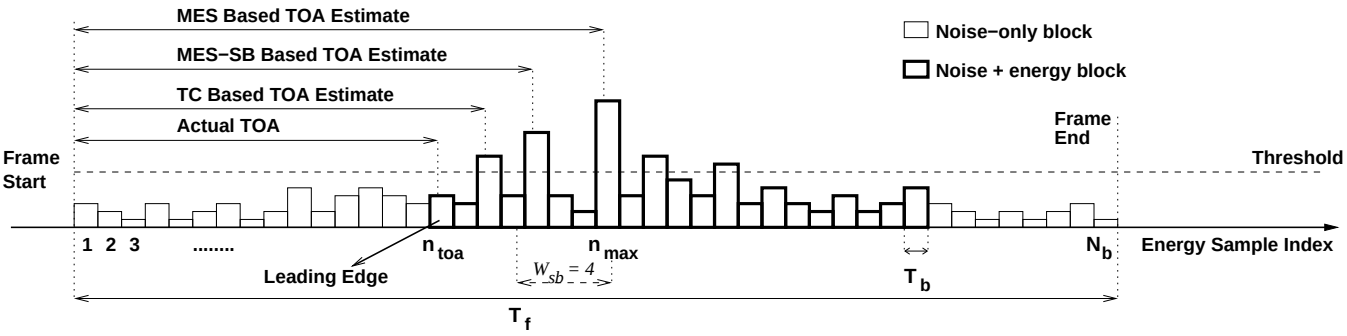

Fig. 3. Illustration of basic TOA estimation techniques based on energy samples.

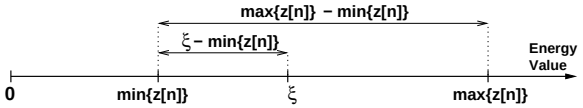

Fig. 4. Illustration of the normalized adaptive threshold depending on the minimum and maximum energy samples.

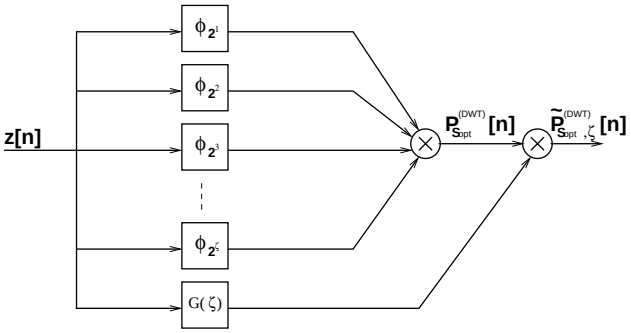

Fig. 5. Block diagram for weighted multi-scale product of MZ-DWT.

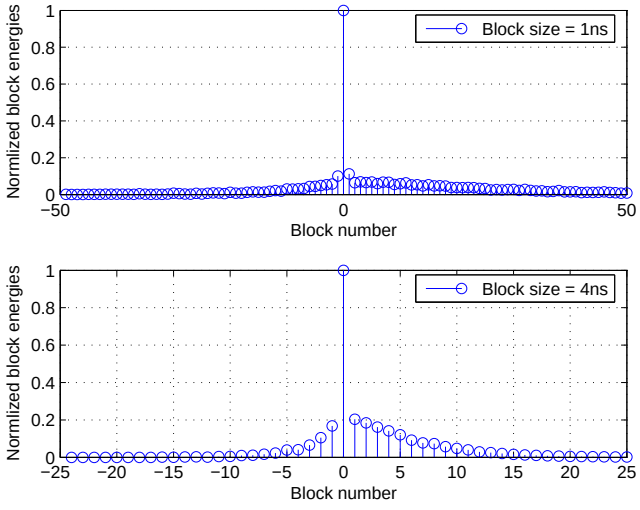

Fig. 6. Mean block energies around the maximum energy block in CM1 for $T_b = 1$ns and 4ns. Samples with negligible values are discarded on the plots. Time reversed forms of these functions are used for filtering the energy vector prior to block detection (F-MES).

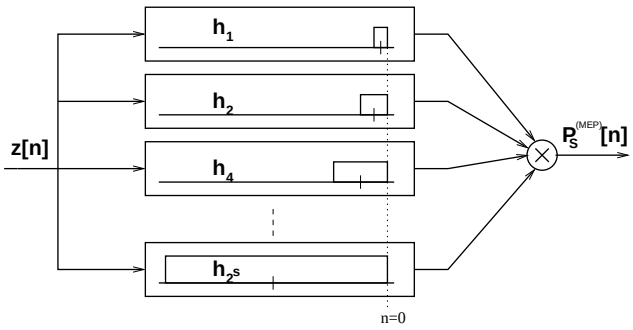

Fig. 7. Filter bank for analyzing the signal energy at different times scales.

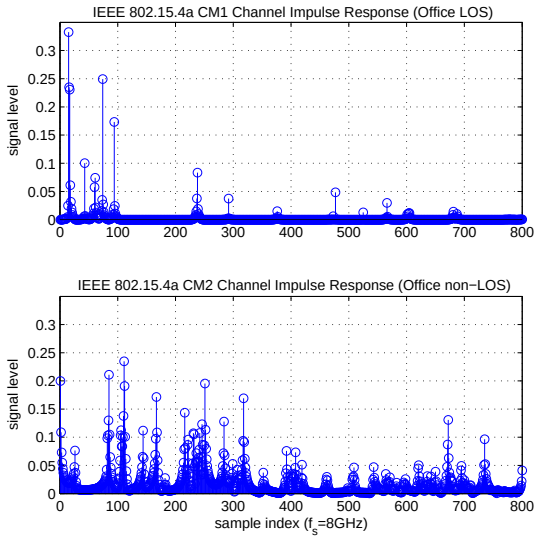

Fig. 8. Typical IEEE 802.15.4a channel impulses in (top) residential LOS (CM1) and (bottom) residential non-LOS (CM2) environments

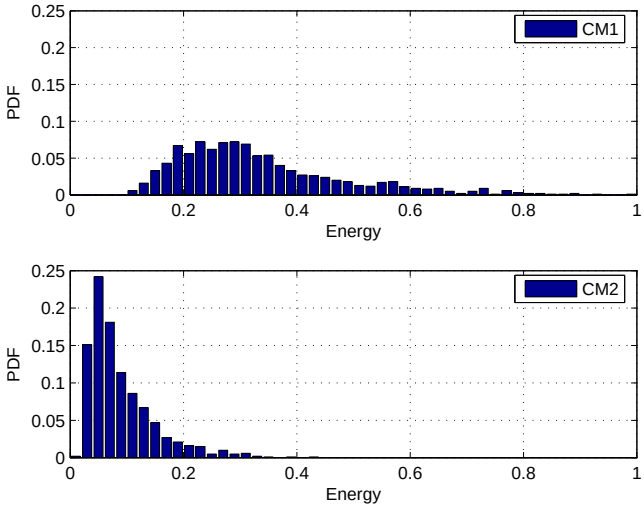

Fig. 9. Comparison of the PDFs of energy of maximum energy block for CM1 and CM2 ($T_b = 1$ns).

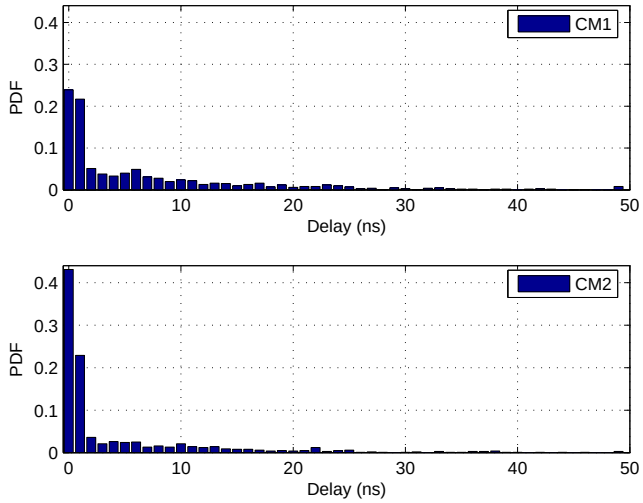

Fig. 10. Comparison of the PDFs of the arrival time of maximum energy block with respect to the first energy block for CM1 and CM2 ($T_b = 1$ns).

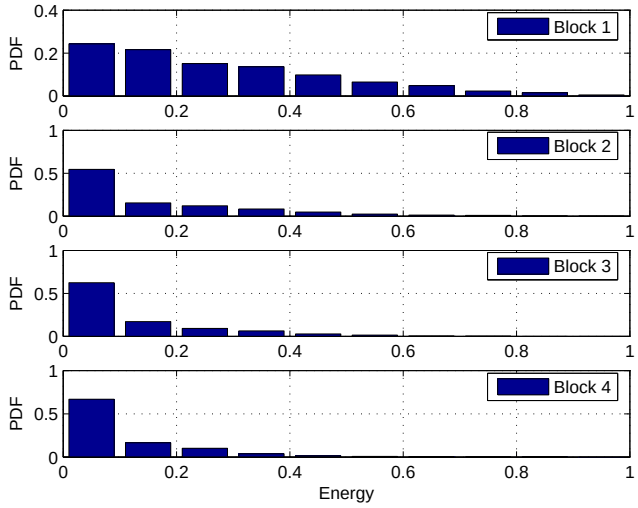

Fig. 11. PDFs of block energies in the first four energy blocks ($T_b = 4$ns). Uniformly distributed delay of the first arriving path within the block interval is considered.

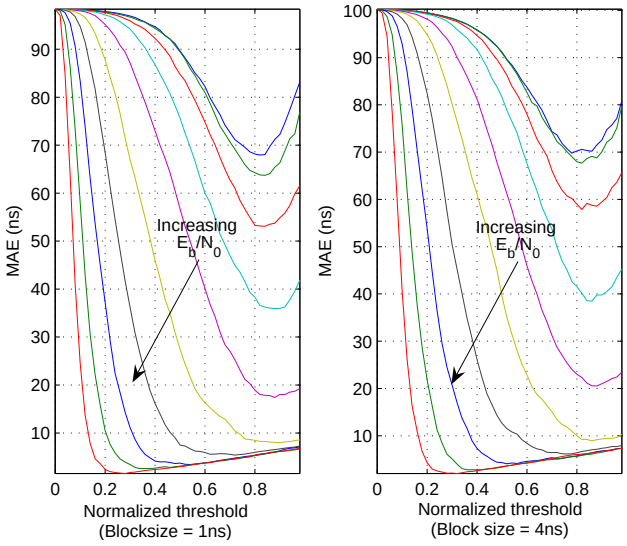

Fig. 12. MAE of TOA estimation under CM1 with respect to the normalized threshold for $E_b/N_0 = \{8, 10, 12, 14, 16, 18, 20, 22, 24, 26\}$dB.

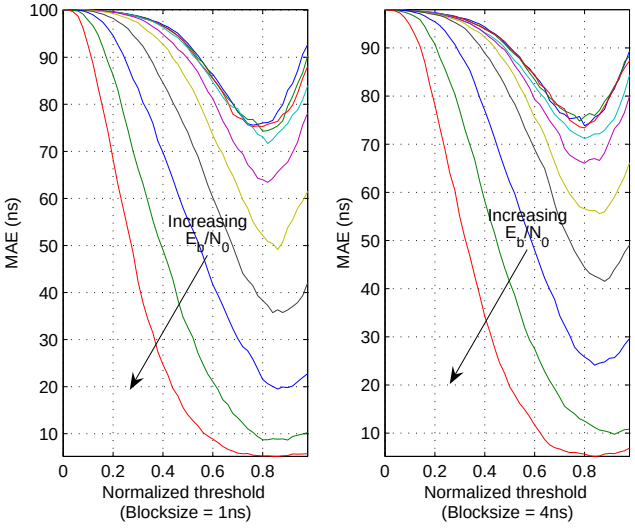

Fig. 13. MAE of TOA estimation under CM2 with respect to the normalized threshold for $E_b/N_0 = \{8, 10, 12, 14, 16, 18, 20, 22, 24, 26\}$dB.

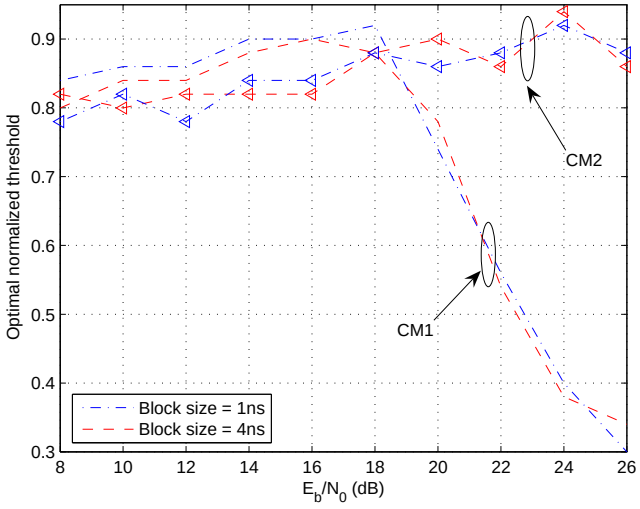

Fig. 14. Optimum normalized thresholds with respect to E_b/N_0 under CM1 and CM2.

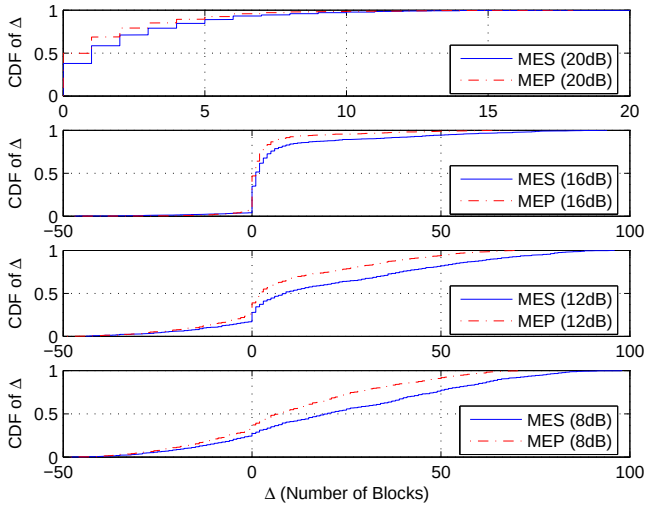

Fig. 15. CDFs of delays between the first energy block and maximum energy block, before and after the bank of multi-scale filters.

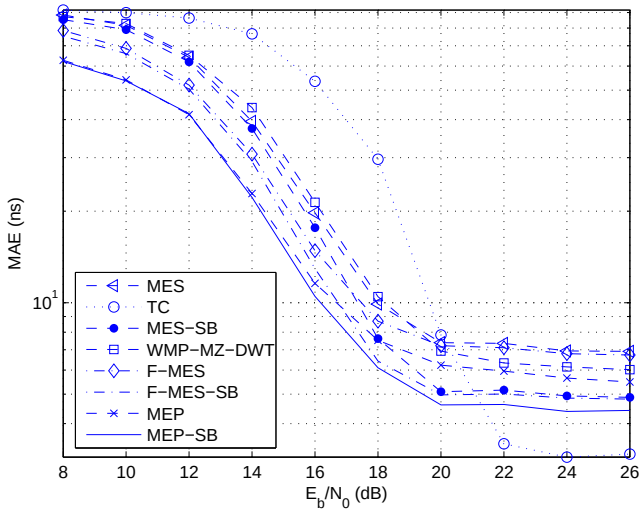

Fig. 16. Absolute error plots for different algorithms with respect to E_b/N_0 (CM1, $T_b = 1$ns).

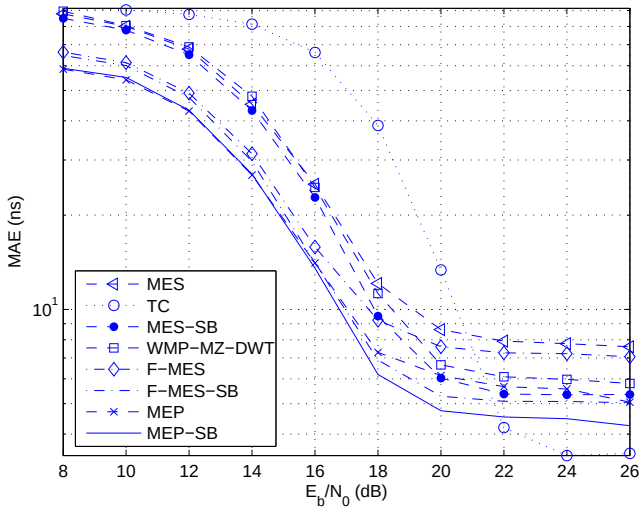

Fig. 17. Absolute error plots for different algorithms with respect to E_b/N_0 (CM1, $T_b = 4$ns).

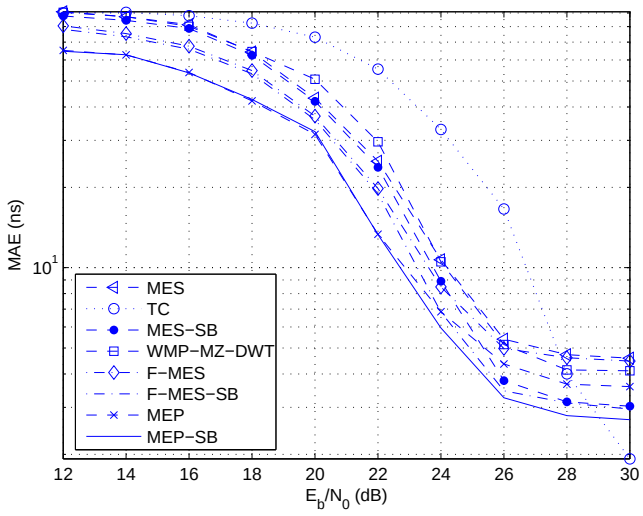

Fig. 18. Absolute error plots for different algorithms with respect to E_b/N_0 (CM2, $T_b = 1$ns).

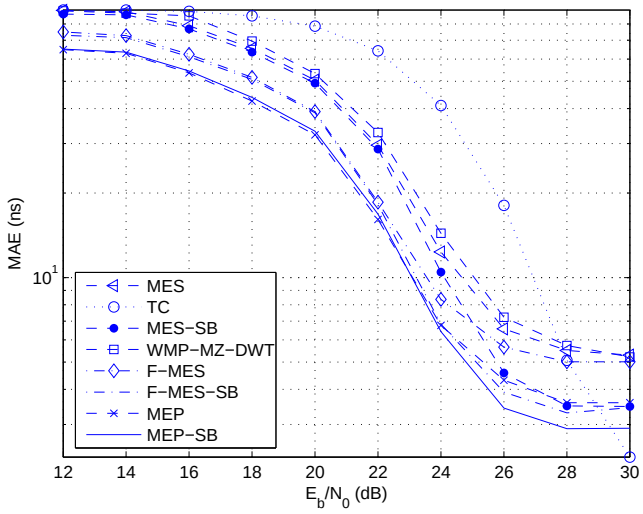

Fig. 19. Absolute error plots for different algorithms with respect to E_b/N_0 (CM2, $T_b = 4$ns).

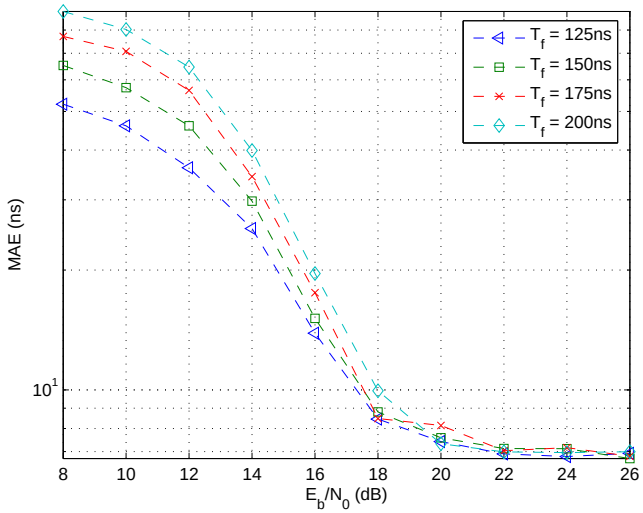

Fig. 20. Effect of number of blocks on the performance of MES (CM1, $T_b = 1$ns).

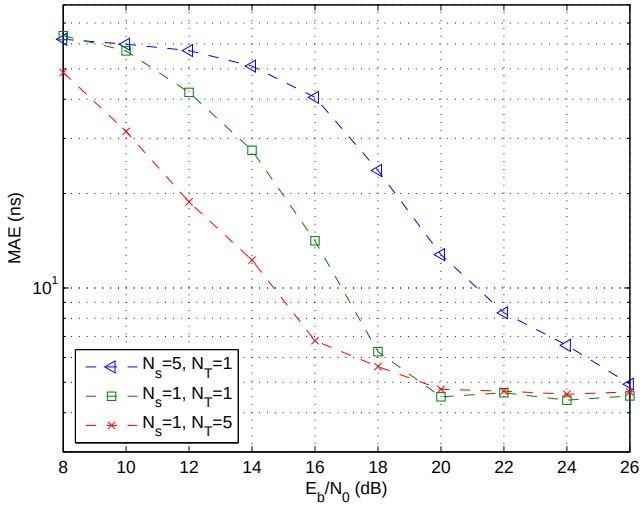

Fig. 21. Comparison of the MAE performance of MES for different N_s and N_T values (CM1, $T_b = 4$ns).

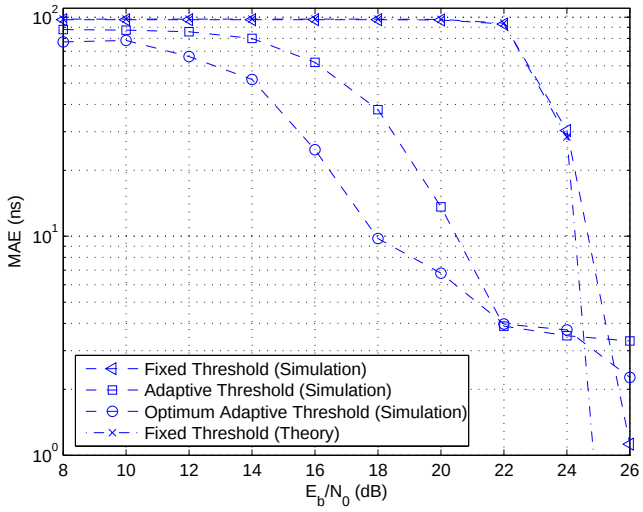

Fig. 22. Comparison of theoretical and simulation results with respect to E_b/N_0 for fixed and adaptive threshold based TOA estimation algorithms (CM1, $T_b = 4$ns).